HHS Public Access

Author manuscript

Ultrasound Med Biol. Author manuscript; available in PMC 2020 August 30.

Published in final edited form as:

Ultrasound Med Biol. 2019 December ; 45(12): 3232–3245. doi:10.1016/j.ultrasmedbio.2019.08.014.

The proteomic effects of pulsed focused ultrasound on tumor microenvironments of murine melanoma and breast cancer models

Omer Aydin[*,a,b], **Rebecca Lorsung**[a], **Parwathy Chandran**[a], **Gadi Cohen**[a], **Scott R. Burks**[a], **Joseph A. Frank**[*,a,c]

[a]Frank Laboratory, Radiology and Imaging Sciences, Clinical Center, National Institutes of Health, Bethesda, MD 20892

[b]Erciyes University, School of Engineering, Department of Biomedical Engineering, 38039, Talas, Kayseri, Turkey

[c]National Institute of Biomedical Imaging and Bioengineering, National Institutes of Health, Bethesda, MD 20892

Abstract

Non-ablative pulsed focused ultrasound (pFUS) targets non-thermal forces that activate local molecular and cellular immune responses. Optimal parameters to stimulate immunotherapeutic anti-tumor microenvironments (TME) and responses in different tumor types remain uninvestigated. Flank B16 murine melanoma and 4T1 breast tumors received 1 MHz pFUS at 1–8MPa peak negative pressure (PNP) and analyzed 24hr post-sonication. Necrosis or hemorrhage were unaltered in both tumors, but pFUS induced DNA strand breaks in tumor cells at PNP ≥6MPa. pFUS at >4MPa suppressed anti-inflammatory cytokines in B16 tumors. pFUS to 4T1 tumors decreased anti-inflammatory cytokines and increased pro-inflammatory cytokines and cell adhesion molecules. pFUS at 6MPa increased calreticulin and alterations check-point proteins along with tumoral and splenic immune cell changes that could be consistent with a shift towards an anti-tumor TME. pFUS-induced TME alterations shows promise in generating anti-tumor immune responses, but non-uniform responses between tumor types require additional investigation to assess pFUS as a suitable anti-tumor therapy.

Keywords

focused ultrasound; tumor microenvironment; melanoma; breast cancer; proteomics; flow cytometry

INTRODUCTION

The tumor microenvironment (TME) consists of cancer cells, stem cells, immune cells, stromal cells, vasculature, and extracellular matrix (ECM) that respond to local molecular

[*]To whom correspondence may be addressed. biomer@umich.edu; jfrank@nih.gov.

The authors have no conflict of interests and nothing to declare.

cues to stimulate cell proliferation, anti-apoptotic signaling, and metastatic spread to other organs (Junttila and de Sauvage 2013). The interrelationship between malignant cells and the immune system arises from cell-cell interactions and the production of cytokines, chemokines and trophic factors (CCTF) that favor either anti-tumor or immunosuppressive (i.e., tolerance) conditions within the TME (Lee and Margolin 2011, Makkouk and Weiner 2015). These interactions and chemotaxis of immune cell tropism is dependent upon CCTF, cell adhesion molecules (CAM) and damaged associated molecular patterns (DAMP) by cellular elements (i.e., tumors, stromal cells and endothelium) in response to therapeutic intervention (Balkwill 2004, Nagarsheth, et al. 2017). Various CCTF act as intra-tumoral immunosuppressants and directly affect recruitment and differentiation of T regulator cells (Treg), myeloid-derived suppressor cells (MDSC), and tumor associated macrophage (TAM). They include transforming growth factor beta (TGFb), interleukins (IL) 4, 10, 13, and vascular endothelial growth factor (VEGF) (Zou 2005). The ability to shift the TME towards an anti-tumor immune environment by decreasing TGFb, IL-10 expression, or increasing DAMPS along with IL1a, IL1b, IL2, IL17, tumor necrosis factor alpha (TNFa), interferon gamma-induced protein 10 (IP10) and interferon gamma (INFg) can lead to infiltration by cytotoxic T cells (Tcyt), T helper cells (Th), dendritic cells (DC), and natural killer cells (NK) that potentiate cytotoxic immune responses (Barker, et al. 2015, Taylor, et al. 2006).

Cellular and biological immunotherapies are being investigated to treat solid tumor malignancies in preclinical models or clinically as part of strategy to enhance antitumor immune responses within the TME (Khalil, et al. 2016). These approaches may not be effective primarily due to the immunosuppressive TME and may require the addition of exogenous such as radiation therapy, radiofrequency ablation, or high intensity focused ultrasound (HIFU) targeted to tumors which could aid in a more robust therapeutic response. (Chew, et al. 2012). The ability to change the TME from an immunosuppressive to cytotoxic, immune anti-tumor environment could impact tumor progression (Whiteside 2008).

Image guided High Intensity Focused Ultrasound (HIFU) is a noninvasive approach used to ablate tumors in patients that may not be eligible for surgical debulking or as a palliative pain treatment (Webb, et al. 2011) (Khokhlova and Hwang 2016). The cellular debris following ablative HIFU has been shown to prime the immune system when used alone or in combination with checkpoint inhibitors and result in an abscopal effect on distant tumors (Silvestrini, et al. 2017). HIFU can induce rapid temperature elevation and protein denaturation within tissues (Hu, et al. 2005, Kim, et al. 2008) and variants of this approach such as boiling histotripsy can vaporize targeted areas stimulating the release of cellular debris and microRNA into the circulation (Chevillet, et al. 2017, Hoogenboom, et al. 2015). HIFU thermal ablation has been shown to induce antitumor immune responses with higher numbers of infiltrating Tcyt, Th, NK cells, proinflammatory macrophages (M1), and DC in the targeted tissues along with release of heat shock proteins (Unga and Hashida 2014, Xu, et al. 2009). In comparison, pFUS techniques that impart primarily mechanical forces to tissues without significant heating. pFUS can alter the integrity of cellular membranes have received limited investigation regarding their potential to induce inflammatory responses within tumors. A potential clinical strategy for utilizing nonthermal pFUS would be to limit

the amount of cellular damage while stimulating an immune response in metastatic disease that would be surrounded by normal tissues.

It has been reported that pFUS to targeted tissues can induce changes in the tissue microenvironment with increased expression of CCTF and CAM that can last for 24-48 hr post-sonication with a total US pressure deposition of 1 second (Burks, et al. 2011, Jang, et al. 2017, Kovacs, et al. 2017, Nguyen, et al. 2015). Image guided pFUS coupled with or without infusion of US microbubble (MB) contrast agent to muscle, heart, and brain has resulted in enhanced stem and immune cell homing to targeted tissues (Alkins, et al. 2013, Burgess, et al. 2011, Burks, et al. 2018, Burks, et al. 2015, Ghanem, et al. 2009, Kovacs, et al. 2017, Kovacs, et al. 2018, Tebebi, et al. 2017, Zen, et al. 2006, Zhong, et al. 2012). Using pFUS to maximize CCTF and CAM alterations in TME that would modulate immunotherapeutic responses have not been thoroughly investigated in different tumors or compared between malignancies of differing cellular origins. In this study, we treated the B16 murine melanoma and 4T1 breast cancer flank tumors with pFUS at 1 MHz over a range of peak negative pressures (PNP) and investigated the effects of sonication on the acute changes in CCTF, CAM, DNA damage and immune cells infiltration in the TME within 24 hours.

MATERIAL AND METHODS

Animals

All animal studies were approved by the Animal Care and Use Committee of the Clinical Center and the procedures were performed according to National Research Council's Guide for the Care and Use of Laboratory (2011). Female C57BL/6 (n=48) and BALB/C (n=48) mice (6-8 weeks old) were purchased from Charles River (Wilmington, MA) and were housed with free access of food and water. Twenty-four hours prior to tumor inoculation or pFUS treatment, hair on both legs was removed with depilatory cream.

Cell Culture

B16, melanoma cells (ATCC, Manassas, VA) were cultured in T-175 flasks using DMEM (Gibco, Life Technologies, Grand Island, NY) supplemented with 10% fetal bovine serum (FBS), 1% Pen Strep (Penicillin Streptomycin, Gibco, Life Technologies, Grand Island, NY). Murine 4T1 breast cancer cells (ATCC, Manassas, VA) were cultured in T-175 flasks in RPMI 1640 (Gibco, Life Technologies, Grand Island, NY) with the same supplements. The cells were maintained at 37°C, 5% CO_2, and 95% relative humidity. The medium was changed every other day and the cells were passaged at 75-90% confluency using TyrpLE Express Enzyme (Gibco, Live Technologies, Grand Island, NY).

Tumor Models

The tumor cells (B16 or 4T1) were harvested from flasks, washed with PBS in the flasks and passaged with 3 mL of TyrpLE and incubated in the incubator for 3-5 min. Afterwards 10 mL of total medium was added to inhibit enzymatic activity and transfer cells from the flask to 15 mL of conical tube. The cells were centrifuged at 1500 rpm for 5 min to collect the cells. 500,000 cells in 100 μL of Dulbecco's phosphate-buffered saline were subcutaneously

inoculated to both flanks of each mouse under anesthesia with 1.5-3% isoflurane in 100% O_2. The health of mice was monitored daily, and the size of tumor was measured externally using digital calipers. Total number of female mice used for this study is n=96. Sample sizes were 5 bilateral-tumor-bearing mice (10 tumors and 5 spleens)/PNP and an identically sized control (PNP=0MPa). pFUS at PNP=6MPa was performed in an additional 5 bilateral-tumor-bearing mice per tumor type (B16 and 4T1) for flow cytometric analysis (FACS) and histology unless otherwise noted. In some cases, there was insufficient tissue to perform following appropriate processing for FAC analysis.

pFUS Treatment

pFUS was administered with a VIFU 2000 (Alpinion Medical Systems, Bothell, WA, www.alpinionusa.com) under ultrasound imaging guidance with an e-Cube 12 (Alpinion) in degassed water at 37 °C. pFUS exposures utilized a 1.15 MHz single-element transducer (8.5 cm in diameter) with a 1.0 mm focal diameter and 7 mm focal depth (3 dB cutoff) using the following peak rarefaction amplitudes of 1, 2, 4, 6, or 8 MPa which corresponded to acoustic powers of 4.6, 9.2, 18.5, 27.7, and 37.0 W, respectively. Sonications used a pulse repetition frequency of 10 Hz with 10 msec US bursts (duty cycle = 10%). Each treatment point received 100 pulses. For treatment planning, the entire tumor was treated using elemental spacing of 2 mm between points. Once the tumor size reached to ~8mm in diameter (~7-10 days) mice were sonicated at the indicated PNP. Mice bearing control tumors received sham pFUS treatments (transducer power = 0 W).

Tissue Harvesting

Twenty-four hours post-pFUS, tumors were harvested for histology, proteomic, and flow cytometric analyses. Mice being euthanized for histological evaluation were perfused through the left ventricle with 10% formalin and harvested tumors were submerged in excess formalin for an additional 24 hours before processing. Tumors for proteomic and flow cytometric analyses were harvested from mice that did not receive vascular perfusion. Tumors for proteomic analyses were frozen in liquid N_2 and stored at −80 °C until further use. Tumors for flow cytometric analyses (FACS) were processed under aseptic conditions. Tumors were minced and enzymatically digested for 60 min in a solution of PBS containing 2% fetal bovine serum, 1% Pen Strep, 1% collagenase at 37°C. Following digestions tumors were mechanically agitated and passed through a 70-μm filter and fixed for 15 min using a solution of 4% paraformaldehyde. Cells were then stored at 4 °C in PBS until flow cytometry. Spleens for FACS were also processed aseptically, where samples were minced, mashed between two frosted glass slides and passed through 70 μm strainers to obtain single cell suspension. Cells were then washed in PBS, fixed using 4% formaldehyde, and stored at 4 °C in PBS until flow cytometry analysis.

Histological Analyses

Tissue was embedded in paraffin, sectioned at a thickness of 5 μm, and mounted onto positively-charged slides. Slides were baked in 65 °C for 1 h and paraffin was removed in xylene. Tissue was rehydrated in graded ethanol and rinsed with distilled water before staining with hematoxylin for 4 min. After thorough washing with tap water, slides were treated with bluing agent for 4 min and washed again in tap water for 1 min. Slides were

rinsed in 95% ethanol and counterstained in eosin solution for 3 min. Slides were dehydrated through graded ethanol, cleared in xylenes, and cover-slipped with Permount (ThermoFisher Scientific, Houston, TX). Three representative sections from each tumor sonicated at the various PNP and control were evaluated qualitatively for hemorrhage and necrosis.

DNA Damage Assay

B16 and 4T1 control (0 MPa), 1 MPa, 2 MPa, 4 MPa, 6 MPa, 8 MPa: Cells fixed for flow cytometry were used in a terminal UTP end-nick ligase (TUNEL) assay to investigate relative cell death response to various treatment pressures (Roche Applied Science, Indianapolis, IN). Cells from 6 tumors (n=3 mice/tumor type) in each treatment group were used. Fixed cells were permeabilized with 0.1% Tritonx-100 in PBS, then incubated with the fluorescein-based TUNEL reaction mixture for 1 h at room temperature. Cells were washed with PBS to remove excess fluorophore. 4’,6-diamidino-2-phenylindole (DAPI, Life Technologies, Carlsbad Ca) was applied for 5 min at a concentration of 1 μg/uL in PBS, and cells were again washed in PBS and transferred into a 96 well plate. Fluorescence intensity of fluorescein (λ_{ex}: 488 nm and λ_{em}: 515 nm) and DAPI (λ_{ex}: 358 nm and λ_{em}: 461 nm) were measured using a SpectraMax M5 plate reader (Molecular Devices, San Jose, CA). Fluorescein fluorescence intensity was then used to normalize the cell concentration in each well (determined using the Cellometer AutoT4 (Nexcelom Bioscience, Lawrence, MA).

DNA damage in cells was also qualitatively assessed histologically using the same fluorescein-based *in situ* cell death TUNEL detection kit (Roche, Mannheim, Germany). Histological paraffin sections were permeabilized using 0.1% Tritonx-100 in PBS and incubated with 100 μL of TUNEL for 1 h at 37 °C. The samples were washed in PBS to remove excess unbounding reactants and coverslips were mounted using Prolong Gold antifade reagent with DAPI (Life Technologies). Five-micrometer sections were imaged with an Aperio ScanScope (Leica Biosystem, Vista, Ca) for the presence of fluorescein-positive nuclei using identical exposure times across tissues. Three sections of each tumor type from n=3 mice per group were qualitatively analyzed to assess patterns of DNA damage.

Proteomic Analyses

Tumor samples were homogenized in cell lysis buffer (PBS + 0.5% Tween-20) containing protease inhibitor cocktail (Roche, Mannheim, Germany) at 4 °C using 1.0 mm Zirconia Beads (Biospect, Bartlesville, OK) using a Mini-bead Beater (Biospect, Bartlesville, OK). Samples were centrifuged twice at 15,000 rpm for 20 min at 4 °C. The supernatant from the second centrifugation used for analysis. Total protein content of each sample was determined using a bicinchoninic acid assay following to manufacturer’s protocol. (Pierce™, Thermo Scientific, Rockford, IL). Cytokine levels for pFUS-treated and untreated tumor were measured using a 32-plex Mouse Cytokine Chemokine Magnetic Bead Panel (MCYTMAG-70-PX32, MILLIPLEX® MAP Kit, Merk Millipore, Lexington, MA) with Bio-Plex 200 System (Bio-Rad, Hercules, California). The assay was performed according to manufacturer’s protocols with each sample at a protein concentration of 2 mg/ml.

The same homogenates were also analyzed by enzyme-linked immunosorbent assays (ELISA) for the following protein levels: intracellular adhesion molecule-1 (ICAM-1),

vascular cell adhesion molecule (VCAM), cyclooxygenase-2 (COX2), TGFb, and TNFa (all from R&D Systems, Minneapolis, MN). All ELISA were performed according to the manufacturers' protocols using a total protein concentration of 2 mg/mL and were read on a spectrophotometric plate reader (Spectra Max M5, Molecular Devices, Sunnyvale, CA).

Flow Cytometry Analysis (FACS)

Due to fixation, live/dead analyses on cells were not performed. For immunostaining, 1 million cells from spleen, or tumor samples were initially treated with Fc-Receptor blocking antibody (purified anti-mouse CD16/32 antibody, BioLegend, San Diego, USA) in antibody staining buffer (0.5% BSA, 2 mM EDTA, 1X PBS) for 10 min at 4°C, to reduce non-specific immunofluorescent staining. Samples were then stained for 45 min on ice, with the following fluorescently-labelled antibodies (Biolegend, San Diego, USA) in antibody staining buffer: FITC anti-mouse CD3 (clone 17A2), FITC anti-mouse F4/80 (clone BM8), FITC anti-mouse CD45 (clone 30-F11), PE anti-mouse CD25 (clone PC61), PE anti-mouse CD8a (clone 53-6.7), PE anti-mouse CD206 (clone C068C2), PE anti-mouse CD19 (clone 1D3/CD19), PE anti-mouse CD11c (clone N418), PE anti-mouse CD11b (clone M1/70), (clone 10F.9G2), APC anti-mouse CD4 (clone RM4-5), APC anti-mouse CD86 (clone GL-1), APC anti-mouse Ly-6G/Ly-6C (Gr-1) (clone RB6-8C5), APC anti-mouse CD152 (clone UC10-4B9), Alexa Fluor® 647 anti-mouse CD335 (NKp46) (clone 29A1.4), and Alexa Fluor® 647 anti-mouse CD279 (PD-1) (clone 29F.1A12). Matched fluorescently-labelled isotype controls for the above antibodies were used. Following staining, the cells were washed with PBS, resuspended in 200 μl PBS, and loaded on to V-shaped 96 well plates for flow cytometric analysis. Flow cytometry data was collected following manufacturer's instructions on a BD Accuri™ C6 Cytometer equipped with BD Accuri™ C-Sampler (BD Biosciences, San Jose, USA). 10,000 events were acquired from each sample. Flow cytometry data was processed using FlowJo (FlowJo LLC, Oregon, USA) software, and statistical analysis was performed using GraphPad Prism (La Jolla, CA, USA).

Data Processing

All data are presented as mean ± standard deviation with Prism 7, GraphPad Software, Inc. (La Jolla, Ca). One-way analysis of variance (ANOVA) was used for multiple comparisons. Unpaired non-parametric t-tests with Mann-Whitney tests was used for comparison for each cell type measured by flow cytometry.

RESULTS

This study examined the acute effects of molecular, histological, and immune cell changes following pFUS at different peak negative pressures in implanted murine B16 melanoma and 4T1 breast cancer tumor models at 24 hr post-sonication. Changes in immune cell populations were also investigated in spleens at 24 hr following pFUS to tumors.

Histological Analysis of Tumors following pFUS

Ultrasound-guided pFUS was administered to B16 and 4T1 flank tumors over the entirety of the tumors at different PNP. Twenty-four hours post pFUS, animals (n=3/tumor type at pFUS PNP) were euthanized, and tumors were harvested for histological examination and

assessed for DNA damage by TUNEL staining. On gross pathology, there were clear differences between the two tumors types; B16 tumors were soft and pliable in consistency, whereas 4T1 tumors were firm and encapsulated. There were no differences between controls and sonicated masses. H&E demonstrated heterogenous cytoarchitecture independent on pFUS PNP used to treat both tumor types when compared to controls. Figure 1 contains examples of H&E sections from the B16 and 4T1 that received pFUS at 6 MPa versus control tumors. There was no consistent pattern of increased hemorrhage or necrosis in either tumor type treated with pFUS over the range of PNPs (1 to 8 MPa) when compared to controls. There was no evidence of thermal injury in B16 or 4T1 tumors sonicated at PNP of 1-8MPa.

Quantitative analysis of TUNEL in the B16 and 4T1 tumors revealed a significant increase (ANOVA, $p<0.05$ with multiple comparison) in the relative positive nuclei at 6 and 8 MPa compared to control and the other sonicated tumors (Figure 2). Examining the representative TUNEL images for both sonicated and controls tumor groups, the areas of positive cells were primarily located surrounding areas of necrosis in each tumor type. These results would suggest that pFUS PNP ≤4 MPa results in changes in tumors without substantial differences in the amounts of TUNEL-positive cells, whereas PNP ≥6 MPa pressures generate was significant differences ($p<0.05$ ANOVA) in the amount of DNA damage between sonicated and control tumors.

Proteomic Responses of Tumors to pFUS

The proteomic response over the range of pFUS PNP in tumors of similar sizes differed for each tumor type and consisted of increased expression of pro-inflammatory (anti-tumor) factors and decreased expression of anti-inflammatory (immunosuppressive) factors. Figure 3 shows the raw data from single and multiplex ELISAs and heat map representing fold changes compared to control tumors (0MPa) for the B16 melanoma. Significantly decreased expression ($p<0.05$ ANOVA) of IL10 and TGFb were detected post-pFUS at PNP ≥2 MPa. In addition, IL12p40 was significantly decreased ($p<0.05$ ANOVA) starting at 1 MPa through 6 MPa and IL12p70, the second part of the heterodimer, was significantly decreased at 6 and 8 MPa. Increased ICAM was observed at 2 and 4 MPa. In this study, TNFa and IFNg were not detected in the control or sonicated B16 tumors at any PNP.

In comparison, sonicating 4T1 tumors responded to increasing PNP pFUS with greater CCTF and CAM changes compared to sham controls with increasing PNP (Figure 4). Increases in IL 1a, IL1b, and TNFa were detected between peak negative pressure (PNP) of 4-8 MPa but were not always significant. The significant increase ($p<0.05$ ANOVA) in IL17 from 2-8 MPa would also support a proinflammatory TME in response to pFUS at increasing PNP. Although IFNg was not found to be significantly different from control the chemokine interferon gamma-induced protein 10 (IP 10 or CXCL10) was elevated from 2-8 MPa which is secreted in response to IFNg by various cell populations within breast cancer (Jin, et al. 2017, Taslimi, et al. 2016). There were also elevations in ICAM detected in 4T1 tumors between 2-6 MPa. RANTES was also significantly elevated at 2, 4, and 8 MPa but demonstrated inconsistent response to pFUS. Moreover, TGFb was significantly decreased ($p<0.05$ ANOVA) between PNP of 4-8 MPa compared to controls. Overall, while the

changes in CCTF and CAM did not linearly correlate with increasing of PNP, pFUS to the 4T1 tumors tended to support an anti-tumor microenvironment. Differential proteomic responses to pFUS occurred between the B16 melanoma and 4T1 breast cancer most likely arises from differences in the TME. More importantly the decreased expression in TGFb following pFUS at PNP between 4-8 MPa was observed in both tumor types compared to sham controls. Sonicating the tumors at PNP ≥ 4 MPa with pFUS shifted the balance from a tumor immunosuppressive towards an anti-tumor immunity microenvironment based on the changes in expression of CCTF (i.e., IL10, TGFb, IL 1, IL17, IP10) and ICAM.

Flow Cytometric Analysis

The quantitative TUNEL fluorescence results at 6 MPa demonstrated increased DNA damage in tumors which could be associated with release of damage associated molecular patterns (DAMPS) and generate chemoattractants for immune cell tropism. Based on this finding along with the decrease in TGFb in the tumors, we decided to evaluate the immune cell populations from the tumors and spleen at 24 hr post sonication. Tumors and spleens were harvested 24 hr post-pFUS and FACS analysis performed (Figure 5, supplemental Figure 1, supplemental Table 1) for immune cell surface markers. The percentage of each cell type per 10,000 counts after excluding side-scatter events were determined.

For B16 melanoma (n=5 mice, i.e., 10 tumors) sonicated at 6 MPa only demonstrated decreased myeloid suppressive cells (MDSC) ($p=0.0022$) following pFUS. However, the effect of sonicating the B16 melanoma at 6 MPa resulted in numerous differences in immune cell populations in the spleen. Th ($p=0.0079$), Tcyt ($p=0.0079$), total macrophages ($F4/80^+$; $p=0.0159$), M1 ($p=0.0317$) and M2 ($p= 0.0397$) macrophages, and DC ($p= 0.0317$) were all significantly elevated, while NK cells ($p=0.0079$) were significantly decreased in the spleen following pFUS at 6 MPa to the tumor. In comparison, 4T1 tumors (n=5 mice, i.e., 10 tumors) treated at 6 MPa, significant decreases ($p<0.02$ unpaired T-test) were detected in Treg, total macrophages ($F4/80^+$), M1 and anti-inflammatory M2 macrophages, and MDSC at 24 hr post-pFUS. There were no significant differences in Th, Tcyt, NK cells or DC in the 4T1 tumor. FACS of the splenic cell population revealed significant increases in MDSC, DC, and Tcyt (all with $p=0.02$). It is possible that the effects of sonicating the tumor directly altered the splenic microenvironment. However, tumor debris and DAMP could enter the circulation and stimulate immune cell proliferation or transmigration from the spleen. The response to pFUS at 6 MPa did not result in an influx of immune cell populations by 24 hr into both tumor types, which may reflect a time delay between sonication and mobilization of these cells in response to the proteomic changes in the TME.

FACS analysis for calreticulin (Cal) in the isolated B16 tumor cells sonicated at 6MPa revealed a significant ($p=0.0027$) albeit small increase compared to control tumors in the surface expression (Figure 6A). pFUS at 6 MPa did not result in differences in PD1 or CTLA4 on B16 tumor cells. In comparison, pFUS at 6MPa in 4T1 tumors (Figure 6B) did result in significant decreases in PD1 ($p= 0.042$) with non-significant trends for decreased CTLA4 ($p=0.051$) and increased calreticulin ($p=0.054$) at 24 hr post sonication. These results suggest that pFUS can alter expression of surface proteins that can have an influence

in the suppression of phagocytic cells or stimulate these cells to engulf cancer cells within the flank tumors.

DISCUSSION

pFUS mechanotransductive effects in tumors have received little attention in part because this approach is not aimed at ablative treatment. The thermal effects of FUS with or without MB have been shown to release tumor debris, DAMPS, and other protein antigens that can stimulate innate and adaptive immune responses within the tumor (Jang et al., 2018; Liu et al., 2012; Silvestrini et al., 2017; Unga et al., 2014; van den Bijgaart et al., 2017; Wu et al., 2007, Xu et al., 2009). In this study the changes proteomic and immune cell numbers in two tumor types following pFUS at 24 hours to determine how sonication acutely alters the TME. The major finding of this study was that similarities and differences in the molecular response to pFUS mechanical forces occur between the two tumor types with regards to increased or decreased expression of CCTF and CAM. Although it may seem obvious that tumor types derived from differing cell origins (i.e., ectoderm, endoderm, or mesoderm) may respond differently to non-ablative pFUS, this observation has not been thoroughly investigated. Overall, sonicating the tumors at PNP>4 MPa resulted in a shift from an immuo-suppressive towards an anti-tumor immunity TME with increase expression of various CCTF, CAM, and immune cell phenotypes within the spleen and tumor. Moreover, the number of cells with DNA damaged (TUNEL +) increased with PNP > 4MPa in both tumor types compared to control.

Malignant TME can be described as either “cold” (immunosuppressive) or “hot” (anti-tumor) based on the CCTF and immune cell activity present (Nagarsheth, et al. 2017) (Figure 7). Cold tumors tend to express immunosuppressive CCTF in TME accompanied by increased infiltration of Treg, M2 macrophages, and MDSC, with few functional DC or antigen presenting cells (APC). In comparison, hot tumors can have increased expression of pro-inflammatory CCTF along with Tcyt, NK cells, Th, Th17 cells, DC and functional APC that could generate an anti-tumor immune response and slow tumor growth. There is most likely a spectrum or heterogeneous distribution of cold and hot phenotypes within a single tumor that contain areas that could have immune-suppressive or anti-tumor molecular profiles. The proteomic pattern of cold tumors exhibit increased expression of TGFb, IL10, IL4, IL13, VEGF, RANTES, MCP1, MCSF along with decreased expression of proinflammatory CCTF (Ben-Baruch 2006, Jiang, et al. 2016, Pitt, et al. 2016). In hot tumors, increased expression of IFNg, IL1a, IL1b, IL2, IL6, IL12, IL17, TNFa, IP10, monokine induced gamma interferon (MIG), and CAMs can vary and contribute to activating an innate immune response. The balance between the two TMEs can be influenced by external physical stimuli. Radiation therapy (RTx) can induce the TME towards an anti-tumor response by causing DNA damage along with increased mixed histocompatibility class I (MHC I), and release of DAMPs that can activate APC to stimulate Tcyt and NK cells and a subsequent inflammatory response (Barrio, et al. 2012, Gameiro, et al. 2016, Jiang, et al. 2016, Reits, et al. 2006). RTx can profoundly alter the TME by increasing oxygenation levels and interstitial pressure along with causing increased expression of Cal on the plasma membrane of tumor cells, resulting in prophagocytic signaling to macrophages and DC activation shifting toward an anti-tumor immune response

(Jiang, et al. 2016, Obeid, et al. 2007, Raghavan, et al. 2013). RTx can also change the CCTF profile within tumors by altering expression of both pro-inflammatory and anti-inflammatory factors that modulate the immune response and shift the balance from a cold to hot tumor (Barker, et al. 2015, Demaria, et al. 2016, Frey, et al. 2017, Lugade, et al. 2005, Vanpouille-Box, et al. 2015).

Low intensity FUS has been shown to induce a stress response in murine B16 melanoma tumor models by altering the CCTF in the draining lymph node along with stimulating an anti-tumor immune cell profile that resulted in slower tumor growth and metastases (Bandyopadhyay, et al. 2016). Low intensity pFUS with MB has been shown to alter TME with transient increases in tumor infiltrating lymphocytes and Tcyt cells that resulted in slowing colon cancer (CT-26) growth in a mouse model (Liu, et al. 2012). Direct injection of MB into melanoma tumors followed by FUS has also been shown to slow tumor growth and increase necrosis due to inertial cavitation effects in the TME (Jang, et al. 2018). High intensity focused ultrasound (HIFU) treatment to breast cancer has been shown to release DAMPs such as heat shock protein 70 and adenosine triphosphate (ATP) from damaged tumor cells that can serve as chemoattractants for DC, which alter the CCTF profile within the TME and inhibit tumor growth (Deng, et al. 2010, Hu, et al. 2005, van den Bijgaart, et al. 2017, Wu, et al. 2007).

In the present study, B16 and 4T1 flank tumors that were targeted with mechanical pFUS at 6 MPa PNP and acutely harvested at 24hrs demonstrated changes in the CCTF and CAM, as well as Cal and PD1 expressions shifting the balance toward a hot TME. There were marked differences in CCTF expression between the B16 and 4T1 tumors following pFUS over the range of PNP. However, the decreased expression of TGFb and IL10 along with increases in ICAM were common to both tumor types. This would suggest that the mechanical effects of pFUS at >4 MPa would influence the anti-tumor microenvironment. The CCTF profile of the TME may contribute to immune cell phenotypes. Some CCTF have dual functions and can either promote or inhibit tumor development and progression depending on intra-tumoral concentrations of various cell populations within the TME (Lin and Karin 2007). TGFb can be expressed by cancer cells, stromal cells, immune cells, and fibroblasts in the TME, and together with IL10 can influence tumor development and growth (Massague 2008). The decreased expression of TGFb and IL10 following pFUS at 6 MPa has been shown to inhibit tumor proliferation. Moreover, sonicating the 4T1 tumors resulted in increases in TNFa, IP10 and IL17 pro-inflammatory factors which influence immune cell influx into the tumor. IP10 is induced by the presence of INFg that plays a pivotal role in stimulating an anti-tumor immune response by directly suppressing tumor cell proliferation, increasing MHC expression and antigen presentation which can lead to cell death along with immune cell infiltration of Tcyt, Th, macrophages and suppression of Treg function (Ivashkiv 2018, Parker, et al. 2016). IFNg can also suppress tumor metabolism, increase production of TNFa and IL6, while suppressing the intra-tumoral IL10 and angiogenesis (Ivashkiv 2018). The increased expression of IP10 in the 4T1 tumors between 2-6 MPa may be the result of increased cytokines such as IL1a, IL1b, and TNFa following pFUS, which can provide the basis for the margination and infiltration of proinflammatory immune cells within the TME, thus contributing to an anti-tumor response (Figenschau, et al. 2018). In comparison, we did not detect consistent increased expression of these pro-inflammatory

CCTF in the B16 melanoma tumors following pFUS at any PNP. Further studies will be required to determine the optimal pFUS parameters for inducing greater CCTF changes in the TME that would result in shifting the cold tumors to a hot phenotype .

FACS analyses to characterize immune cell profiles in tumors and spleens were performed to compare to proteomic changes in the pFUS-treated tumors of ~8 mm in diameter. pFUS at 6 MPa was selected to sonicate tumors for FACS analysis because we observed changes in DNA damage by TUNEL staining at that PNP which could contribute to the innate and adaptive immune response in the mouse. However, the immune cell profiles within each tumor type and corresponding spleens were not consistently influenced by pFUS at 6 MPa at 24 hr. In the 4T1 tumors (Figure 5), pFUS decreased Treg, F4/80, M1 and M2 macrophages, and MDSC within the 4T1 TME without significantly altering the percentage in NK, Tcyt, or Th cells. In the spleen of these mice, increased detection of Tcyt, DC, and MDSC, while NK cells were decreased which may suggest that the spleen reacting to a possible increase in tumor antigen load within the circulation. In comparison, pFUS at 6 MPa resulted in a decrease in percent of MDSC but without other significant changes. However, in the spleen, Tcyt, Th, F4/80, M1, and M2 macrophages, and DC percentages were increased suggesting that the spleen was reacting to tumor antigens within the systemic environment. The mechanisms behind pFUS decreasing MDSC within the B16 tumors remain unclear. Changes in MDSC populations can be altered by the administration of cytotoxic drugs (Suzuki, et al. 2005, Vincent, et al. 2010, Zollo, et al. 2012). The decrease in macrophages following pFUS at 6MPa in the 4T1 tumors is different than what has previously been reported in the literature following ablative sonication (Lu, et al. 2009, Shin, et al. 2018, Silvestrini, et al. 2017). One major difference between studies that report increased macrophage populations in breast cancer following ablative HIFU and the current study aside from the ultrasound modality employed, is the time the tissue was harvested (i.e., 2-14 days post sonication). It is possible that the increased tropism of monocytes/macrophages to sonicated tumors requires >24 hours and we plan to investigate longer followup after a single or multiple nonablative pFUS sonications to the tumors to further understand the immune response. The lack of changes in immune cell populations within the B16 tumor may reflect the relative changes in CCTF and CAM following pFUS. In 4T1 and to a lesser extent in B16 tumors, we observed pFUS decreased CTLA4 and PD1, while increasing Cal. These changes presumably induced in the TME may provide a synergistic effect where cancer cell engulfment by antigen presenting cells (APC) such as DC and macrophages acts in combination with CCTF changes in the TME to enhance immune cell infiltration that would inhibit tumor growth and invasion (Chao, et al. 2010, Liu, et al. 2015, Obeid, et al. 2007, Willingham, et al. 2012). Our approach could be used for targeting satellite micro-metastatic disease in normal tissues to induce a CCTF and CAM response on endothelium increase tropism of immune cells to lesions. Moreover, non-ablative pFUS could be include as an adjunct by treating tumor margins following ablative therapy, especially if tumor margins need to be left because of sensitive tissues or anatomical location. This approach would be readily translatable to clinical trial requiring the additional time to circumscribe ablative regions with nondestructive pFUS. Since non-ablative pFUS at ~6MPa and parameters used in this study does not cause tissue damage, it maybe also possible to perform repeated treatments that could have positive influence on immune surveillance in

treating satellite tumors. The increase in CCTF, CAM and DNA damage could further stimulate greater innate and adaptive immune responses in surrounding tissues where micro-metastatic disease would normally go untreated. This approach may also improve other types of therapy such as using check point inhibitors with pFUS either before or after ablative approaches to drive the immune system (Silvestrini, et al. 2017). The results of this study demonstrate the importance of evaluating the molecular responses exposed to pFUS with increasing mechanical forces in different tumor types and evaluate the acute changes in CCTF, CAM and immune cell population. Further investigation into the mechanotransductive effects of mechanical pFUS in different solid tumors especially in regards to the molecular and immune responses that could be generated and exploited in the treatment of diseases.

There are some limitations of this study that need to be addressed. The proteomic and immune cell response to pFUS was performed on tumors ~8mm in diameter and were harvested 24 hr later. It is unknown if tumor size prior to pFUS may influence expression of DAMPs, CCTF, and CAM or immune cell response. It is possible the TME CCTF and CAM changes could evolve with growth and size such that the tumor shifts from hot to cold and becomes less responsive to the mechanical effects of pFUS. Sampling the tumors earlier or days later post-pFUS may result in different proteomic or immune cell profiles. The fact that an influx of immune cell populations was not observed in both tumor types by 24 hr warrants further investigation into the temporal responses, which may help understand potential delays between sonication and mobilization of these cells in response to the proteomic changes in the TME. However, this was beyond the immediate scope of the present study. In addition, the effect of age and gender on proteomic and immune cell profile response would also need to be investigated. Further research investigating the changes in CCTF and CAM in tumors over time without intervention may provide a basis for the type and magnitude of anti-tumor immune response that can be generated by non-ablative pFUS. The proteomic response presented in this study is limited in breath or sampling with emphasis primarily on acute time point following pFUS. A broader interrogation into proteomic changes as well as performing transcriptomic analysis of the two tumor types in order to further evaluate similarities or differences in response to non-ablative pFUS.

Another limitation was the inability to measure cell viability (i.e., distinguish live versus dead cells) with FACS in cell populations detected in the two tumor types. The numbers of tissue samples harvested and 15 cell surface markers per tumor evaluated required that cells be fixed and analyzed by FACS over subsequent days. Moreover, we were only able to perform FACS analysis for immune cell populations on cells isolated from tumors and spleens, not regional lymph nodes, following pFUS at 6 MPa at 24 hr due to limitation of available tissue for processing. Future studies should assess changes in the immune cell profiles following sonication to define a clearer understanding of the directional trafficking of immune cells between the spleen, lymph nodes, and tumors. Lastly, the changes in TME described in response to pFUS may only be applicable to the flank tumors for 4T1 breast cancer or B16 melanoma metastasis and that the growth pattern and CCTF, CAM and immune cell profile could be different in other organs (Taube, et al. 2018).

Supplementary Material

Refer to Web version on PubMed Central for supplementary material.

Acknowledgment and funding:

This work was supported by the Intramural Research Programs of the Clinical Center and of the National Institute of Biomedical Imaging and Bioengineering at the National Institutes of Health.

References

In: th, ed. Guide for the Care and Use of Laboratory Animals. Washington (DC), 2011.

Alkins R, Burgess A, Ganguly M, Francia G, Kerbel R, Wels WS, Hynynen K. Focused ultrasound delivers targeted immune cells to metastatic brain tumors. Cancer Res 2013; 73:1892–9. [PubMed: 23302230]

Balkwill F. Cancer and the chemokine network. Nat Rev Cancer 2004; 4:540–50. [PubMed: 15229479]

Bandyopadhyay S, Quinn TJ, Scandiuzzi L, Basu I, Partanen A, Tome WA, Macian F, Guha C. Low-Intensity Focused Ultrasound Induces Reversal of Tumor-Induced T Cell Tolerance and Prevents Immune Escape. J Immunol 2016; 196:1964–76. [PubMed: 26755821]

Barker HE, Paget JT, Khan AA, Harrington KJ. The tumour microenvironment after radiotherapy: mechanisms of resistance and recurrence. Nat Rev Cancer 2015; 15:409–25. [PubMed: 26105538]

Barrio MM, Abes R, Colombo M, Pizzurro G, Boix C, Roberti MP, Gelize E, Rodriguez-Zubieta M, Mordoh J, Teillaud JL. Human macrophages and dendritic cells can equally present MART-1 antigen to CD8(+) T cells after phagocytosis of gamma-irradiated melanoma cells. PloS one 2012; 7:e40311. [PubMed: 22768350]

Ben-Baruch A. Inflammation-associated immune suppression in cancer: the roles played by cytokines, chemokines and additional mediators. Semin Cancer Biol 2006; 16:38–52. [PubMed: 16139507]

Burgess A, Ayala-Grosso CA, Ganguly M, Jordao JF, Aubert I, Hynynen K. Targeted delivery of neural stem cells to the brain using MRI-guided focused ultrasound to disrupt the blood-brain barrier. PLOS ONE 2011; 6:e27877. [PubMed: 22114718]

Burks SR, Nagle ME, Bresler MN, Kim SJ, Star RA, Frank JA. Mesenchymal stromal cell potency to treat acute kidney injury increased by ultrasound-activated interferon-gamma/interleukin-10 axis. J Cell Mol Med 2018; 22:6015–25. [PubMed: 30216653]

Burks SR, Nguyen BA, Tebebi PA, Kim SJ, Bresler MN, Ziadloo A, Street JM, Yuen PS, Star RA, Frank JA. Pulsed focused ultrasound pretreatment improves mesenchymal stromal cell efficacy in preventing and rescuing established acute kidney injury in mice. Stem Cells 2015; 33:1241–53. [PubMed: 25640064]

Burks SR, Ziadloo A, Hancock HA, Chaudhry A, Dean DD, Lewis BK, Frenkel V, Frank JA. Investigation of Cellular and Molecular Responses to Pulsed Focused Ultrasound in a Mouse Model. PLOS ONE 2011; 6:e24730. [PubMed: 21931834]

Chao MP, Jaiswal S, Weissman-Tsukamoto R, Alizadeh AA, Gentles AJ, Volkmer J, Weiskopf K, Willingham SB, Raveh T, Park CY, Majeti R, Weissman IL. Calreticulin is the dominant pro-phagocytic signal on multiple human cancers and is counterbalanced by CD47. Sci Transl Med 2010; 2:63ra94.

Chevillet JR, Khokhlova TD, Giraldez MD, Schade GR, Starr F, Wang YN, Gallichotte EN, Wang K, Hwang JH, Tewari M. Release of Cell-free MicroRNA Tumor Biomarkers into the Blood Circulation with Pulsed Focused Ultrasound: A Noninvasive, Anatomically Localized, Molecular Liquid Biopsy. Radiology 2017; 283:158–67. [PubMed: 27802108]

Chew V, Toh HC, Abastado JP. Immune microenvironment in tumor progression: characteristics and challenges for therapy. J Oncol 2012; 2012:608406. [PubMed: 22927846]

Demaria S, Coleman CN, Formenti SC. Radiotherapy: Changing the Game in Immunotherapy. Trends Cancer 2016; 2:286–94. [PubMed: 27774519]

Deng J, Zhang Y, Feng J, Wu F. Dendritic cells loaded with ultrasound-ablated tumour induce in vivo specific antitumour immune responses. Ultrasound Med Biol 2010; 36:441–8. [PubMed: 20172447]

Figenschau SL, Knutsen E, Urbarova I, Fenton C, Elston B, Perander M, Mortensen ES, Fenton KA. ICAM1 expression is induced by proinflammatory cytokines and associated with TLS formation in aggressive breast cancer subtypes. Scientific Reports 2018; 8:11720. [PubMed: 30082828]

Frey B, Ruckert M, Deloch L, Ruhle PF, Derer A, Fietkau R, Gaipl US. Immunomodulation by ionizing radiation-impact for design of radio-immunotherapies and for treatment of inflammatory diseases. Immunol Rev 2017; 280:231–48. [PubMed: 29027224]

Gameiro SR, Malamas AS, Bernstein MB, Tsang KY, Vassantachart A, Sahoo N, Tailor R, Pidikiti R, Guha CP, Hahn SM, Krishnan S, Hodge JW. Tumor Cells Surviving Exposure to Proton or Photon Radiation Share a Common Immunogenic Modulation Signature, Rendering Them More Sensitive to T Cell-Mediated Killing. Int J Radiat Oncol Biol Phys 2016; 95:120–30. [PubMed: 27084634]

Ghanem A, Steingen C, Brenig F, Funcke F, Bai ZY, Hall C, Chin CT, Nickenig G, Bloch W, Tiemann K. Focused ultrasound-induced stimulation of microbubbles augments site-targeted engraftment of mesenchymal stem cells after acute myocardial infarction. Journal of Molecular and Cellular Cardiology 2009; 47:411–8. [PubMed: 19540842]

Hoogenboom M, Eikelenboom D, den Brok MH, Heerschap A, Futterer JJ, Adema GJ. Mechanical high-intensity focused ultrasound destruction of soft tissue: working mechanisms and physiologic effects. Ultrasound Med Biol 2015; 41:1500–17. [PubMed: 25813532]

Hu Z, Yang XY, Liu Y, Morse MA, Lyerly HK, Clay TM, Zhong P. Release of endogenous danger signals from HIFU-treated tumor cells and their stimulatory effects on APCs. Biochem Biophys Res Commun 2005; 335:124–31. [PubMed: 16055092]

Ivashkiv LB. IFNγ: signalling, epigenetics and roles in immunity, metabolism, disease and cancer immunotherapy. Nature Reviews Immunology 2018; 18:545–58.

Jang KW, Seol D, Ding L, Lim TH, Frank JA, Martin JA. Ultrasound-Mediated Microbubble Destruction Suppresses Melanoma Tumor Growth. Ultrasound Med Biol 2018; 44:831–39. [PubMed: 29361373]

Jang KW, Tu T-W, Nagle ME, Lewis BK, Burks SR, Frank JA. Molecular and histological effects of MR-guided pulsed focused ultrasound to the rat heart. Journal of Translational Medicine 2017; 15:252. [PubMed: 29237455]

Jiang W, Chan CK, Weissman IL, Kim BYS, Hahn SM. Immune Priming of the Tumor Microenvironment by Radiation. Trends Cancer 2016; 2:638–45. [PubMed: 28741502]

Jin WJ, Kim B, Kim D, Park Choo HY, Kim HH, Ha H, Lee ZH. NF-kappaB signaling regulates cell-autonomous regulation of CXCL10 in breast cancer 4T1 cells. Exp Mol Med 2017; 49:e295. [PubMed: 28209986]

Junttila MR, de Sauvage FJ. Influence of tumour micro-environment heterogeneity on therapeutic response. Nature 2013; 501:346–54. [PubMed: 24048067]

Khalil DN, Smith EL, Brentjens RJ, Wolchok JD. The future of cancer treatment: immunomodulation, CARs and combination immunotherapy. Nat Rev Clin Oncol 2016; 13:273–90. [PubMed: 26977780]

Khokhlova TD, Hwang JH. HIFU for Palliative Treatment of Pancreatic Cancer. Adv Exp Med Biol 2016; 880:83–95. [PubMed: 26486333]

Kim YS, Rhim H, Choi MJ, Lim HK, Choi D. High-intensity focused ultrasound therapy: an overview for radiologists. Korean J Radiol 2008; 9:291–302. [PubMed: 18682666]

Kovacs ZI, Kim S, Jikaria N, Qureshi F, Milo B, Lewis BK, Bresler M, Burks SR, Frank JA. Disrupting the blood-brain barrier by focused ultrasound induces sterile inflammation. Proc Natl Acad Sci U S A 2017; 114:E75–E84. [PubMed: 27994152]

Kovacs ZI, Kim S, Jikaria N, Qureshi F, Milo B, Lewis BK, Bresler M, Burks SR, Frank JA. Disrupting the blood–brain barrier by focused ultrasound induces sterile inflammation. Proceedings of the National Academy of Sciences 2017; 114:E75–E84.

Kovacs ZI, Tu TW, Sundby M, Qureshi F, Lewis BK, Jikaria N, Burks SR, Frank JA. MRI and histological evaluation of pulsed focused ultrasound and microbubbles treatment effects in the brain. Theranostics 2018; 8:4837–55. [PubMed: 30279741]

Lee S, Margolin K. Cytokines in cancer immunotherapy. Cancers (Basel) 2011; 3:3856–93. [PubMed: 24213115]

Lin WW, Karin M. A cytokine-mediated link between innate immunity, inflammation, and cancer. J Clin Invest 2007; 117:1175–83. [PubMed: 17476347]

Liu H-L, Hsieh H-Y, Lu L-A, Kang C-W, Wu M-F, Lin C-Y. Low-pressure pulsed focused ultrasound with microbubbles promotes an anticancer immunological response. Journal of Translational Medicine 2012; 10:221. [PubMed: 23140567]

Liu X, Pu Y, Cron K, Deng L, Kline J, Frazier WA, Xu H, Peng H, Fu YX, Xu MM. CD47 blockade triggers T cell-mediated destruction of immunogenic tumors. Nat Med 2015; 21:1209–15. [PubMed: 26322579]

Lu P, Zhu XQ, Xu ZL, Zhou Q, Zhang J, Wu F. Increased infiltration of activated tumor-infiltrating lymphocytes after high intensity focused ultrasound ablation of human breast cancer. Surgery 2009; 145:286–93. [PubMed: 19231581]

Lugade AA, Moran JP, Gerber SA, Rose RC, Frelinger JG, Lord EM. Local radiation therapy of B16 melanoma tumors increases the generation of tumor antigen-specific effector cells that traffic to the tumor. J Immunol 2005; 174:7516–23. [PubMed: 15944250]

Makkouk A, Weiner GJ. Cancer immunotherapy and breaking immune tolerance: new approaches to an old challenge. Cancer Res 2015; 75:5–10. [PubMed: 25524899]

Massague J. TGFbeta in Cancer. Cell 2008; 134:215–30. [PubMed: 18662538]

Nagarsheth N, Wicha MS, Zou W. Chemokines in the cancer microenvironment and their relevance in cancer immunotherapy. Nat Rev Immunol 2017; 17:559–72. [PubMed: 28555670]

Nguyen B, Burks S, Kim S, Bresler M, Tebebi P, Frank J. Pulsed focused ultrasound enhances mesenchymal stem cell homing to skeletal muscle in a murine model of muscular dystrophy and homing was suppressed by Ibuprofen. Journal of Therapeutic Ultrasound 2015; 3:P69.

Obeid M, Tesniere A, Ghiringhelli F, Fimia GM, Apetoh L, Perfettini JL, Castedo M, Mignot G, Panaretakis T, Casares N, Metivier D, Larochette N, van Endert P, Ciccosanti F, Piacentini M, Zitvogel L, Kroemer G. Calreticulin exposure dictates the immunogenicity of cancer cell death. Nat Med 2007; 13:54–61. [PubMed: 17187072]

Parker BS, Rautela J, Hertzog PJ. Antitumour actions of interferons: implications for cancer therapy. Nat Rev Cancer 2016; 16:131–44. [PubMed: 26911188]

Pitt JM, Marabelle A, Eggermont A, Soria JC, Kroemer G, Zitvogel L. Targeting the tumor microenvironment: removing obstruction to anticancer immune responses and immunotherapy. Ann Oncol 2016; 27:1482–92. [PubMed: 27069014]

Raghavan M, Wijeyesakere SJ, Peters LR, Del Cid N. Calreticulin in the immune system: ins and outs. Trends Immunol 2013; 34:13–21. [PubMed: 22959412]

Reits EA, Hodge JW, Herberts CA, Groothuis TA, Chakraborty M, Wansley EK, Camphausen K, Luiten RM, de Ru AH, Neijssen J, Griekspoor A, Mesman E, Verreck FA, Spits H, Schlom J, van Veelen P, Neefjes JJ. Radiation modulates the peptide repertoire, enhances MHC class I expression, and induces successful antitumor immunotherapy. J Exp Med 2006; 203:1259–71. [PubMed: 16636135]

Shin SH, Park SH, Kim SW, Kim M, Kim D. Fluorine MR Imaging Monitoring of Tumor Inflammation after High-Intensity Focused Ultrasound Ablation. Radiology 2018;287:476–484. [PubMed: 29369752]

Silvestrini MT, Ingham ES, Mahakian LM, Kheirolomoom A, Liu Y, Fite BZ, Tam SM, Tucci ST, Watson KD, Wong AW, Monjazeb AM, Hubbard NE, Murphy WJ, Borowsky AD, Ferrara KW. Priming is key to effective incorporation of image-guided thermal ablation into immunotherapy protocols. JCI Insight 2017; 2:e90521. [PubMed: 28352658]

Suzuki E, Kapoor V, Jassar AS, Kaiser LR, Albelda SM. Gemcitabine selectively eliminates splenic Gr-1+/CD11b+ myeloid suppressor cells in tumor-bearing animals and enhances antitumor immune activity. Clin Cancer Res 2005;11:6713–21. [PubMed: 16166452]

Taslimi Y, Zahedifard F, Habibzadeh S, Taheri T, Abbaspour H, Sadeghipour A, Mohit E, Rafati S. Antitumor Effect of IP-10 by Using Two Different Approaches: Live Delivery System and Gene Therapy. J Breast Cancer 2016; 19:34–44. [PubMed: 27066094]

Taube JM, Galon J, Sholl LM, Rodig SJ, Cottrell TR, Giraldo NA, Baras AS, Patel SS, Anders RA, Rimm DL, Cimino-Mathews A. Implications of the tumor immune microenvironment for staging and therapeutics. Mod Pathol 2018; 31:214–34. [PubMed: 29192647]

Taylor A, Verhagen J, Blaser K, Akdis M, Akdis CA. Mechanisms of immune suppression by interleukin-10 and transforming growth factor-beta: the role of T regulatory cells. Immunology 2006; 117:433–42. [PubMed: 16556256]

Tebebi PA, Kim SJ, Williams RA, Milo B, Frenkel V, Burks SR, Frank JA. Improving the therapeutic efficacy of mesenchymal stromal cells to restore perfusion in critical limb ischemia through pulsed focused ultrasound. Scientific Reports 2017; 7:41550. [PubMed: 28169278]

Unga J, Hashida M. Ultrasound induced cancer immunotherapy. Adv Drug Deliv Rev 2014; 72:144–53. [PubMed: 24680708]

van den Bijgaart RJ, Eikelenboom DC, Hoogenboom M, Futterer JJ, den Brok MH, Adema GJ. Thermal and mechanical high-intensity focused ultrasound: perspectives on tumor ablation, immune effects and combination strategies. Cancer Immunol Immunother 2017; 66:247–58. [PubMed: 27585790]

Vanpouille-Box C, Diamond JM, Pilones KA, Zavadil J, Babb JS, Formenti SC, Barcellos-Hoff MH, Demaria S. TGFbeta Is a Master Regulator of Radiation Therapy-Induced Antitumor Immunity. Cancer Res 2015; 75:2232–42. [PubMed: 25858148]

Vincent J, Mignot G, Chalmin F, Ladoire S, Bruchard M, Chevriaux A, Martin F, Apetoh L, Rébé C, Ghiringhelli F. 5-Fluorouracil selectively kills tumor-associated myeloid-derived suppressor cells resulting in enhanced T cell-dependent antitumor immunity. Cancer Res 2010;70:3052–61. [PubMed: 20388795]

Webb H, Lubner MG, Hinshaw JL. Thermal Ablation. Seminars in Roentgenology 2011; 46:133–41. [PubMed: 21338838]

Whiteside TL. The tumor microenvironment and its role in promoting tumor growth. Oncogene 2008; 27:5904–12. [PubMed: 18836471]

Willingham SB, Volkmer J-P, Gentles AJ, Sahoo D, Dalerba P, Mitra SS, Wang J, Contreras-Trujillo H, Martin R, Cohen JD, Lovelace P, Scheeren FA, Chao MP, Weiskopf K, Tang C, Volkmer AK, Naik TJ, Storm TA, Mosley AR, Edris B, Schmid SM, Sun CK, Chua M-S, Murillo O, Rajendran P, Cha AC, Chin RK, Kim D, Adorno M, Raveh T, Tseng D, Jaiswal S, Enger PØ, Steinberg GK, Li G, So SK, Majeti R, Harsh GR, van de Rijn M, Teng NNH, Sunwoo JB, Alizadeh AA, Clarke MF, Weissman IL. The CD47-signal regulatory protein alpha (SIRPa) interaction is a therapeutic target for human solid tumors. Proceedings of the National Academy of Sciences 2012; 109:6662–67.

Wu F, Wang ZB, Cao YD, Zhou Q, Zhang Y, Xu ZL, Zhu XQ. Expression of tumor antigens and heat-shock protein 70 in breast cancer cells after high-intensity focused ultrasound ablation. Ann Surg Oncol 2007; 14:1237–42. [PubMed: 17187168]

Xu ZL, Zhu XQ, Lu P, Zhou Q, Zhang J, Wu F. Activation of tumor-infiltrating antigen presenting cells by high intensity focused ultrasound ablation of human breast cancer. Ultrasound Med Biol 2009; 35:50–7. [PubMed: 18950932]

Zen K, Okigaki M, Hosokawa Y, Adachi Y, Nozawa Y, Takamiya M, Tatsumi T, Urao N, Tateishi K, Takahashi T, Matsubara H. Myocardium-targeted delivery of endothelial progenitor cells by ultrasound-mediated microbubble destruction improves cardiac function via an angiogenic response. Journal of Molecular and Cellular Cardiology 2006; 40:799–809. [PubMed: 16678200]

Zhong S, Shu S, Wang Z, Luo J, Zhong W, Ran H, Zheng Y, Yin Y, Ling Z. Enhanced homing of mesenchymal stem cells to the ischemic myocardium by ultrasound-targeted microbubble destruction. Ultrasonics 2012; 52:281–6. [PubMed: 21937069]

Zollo M, Di Dato V, Spano D, De Martino D, Liguori L, Marino N, Vastolo V, Navas L, Garrone B, Mangano G, Biondi G, Guglielmotti A. Targeting monocyte chemotactic protein-1 synthesis with bindarit induces tumor regression in prostate and breast cancer animal models. Clin Exp Metastasis 2012;29:585–601. [PubMed: 22484917]

Zou W. Immunosuppressive networks in the tumour environment and their therapeutic relevance. Nat Rev Cancer 2005; 5:263–74. [PubMed: 15776005]

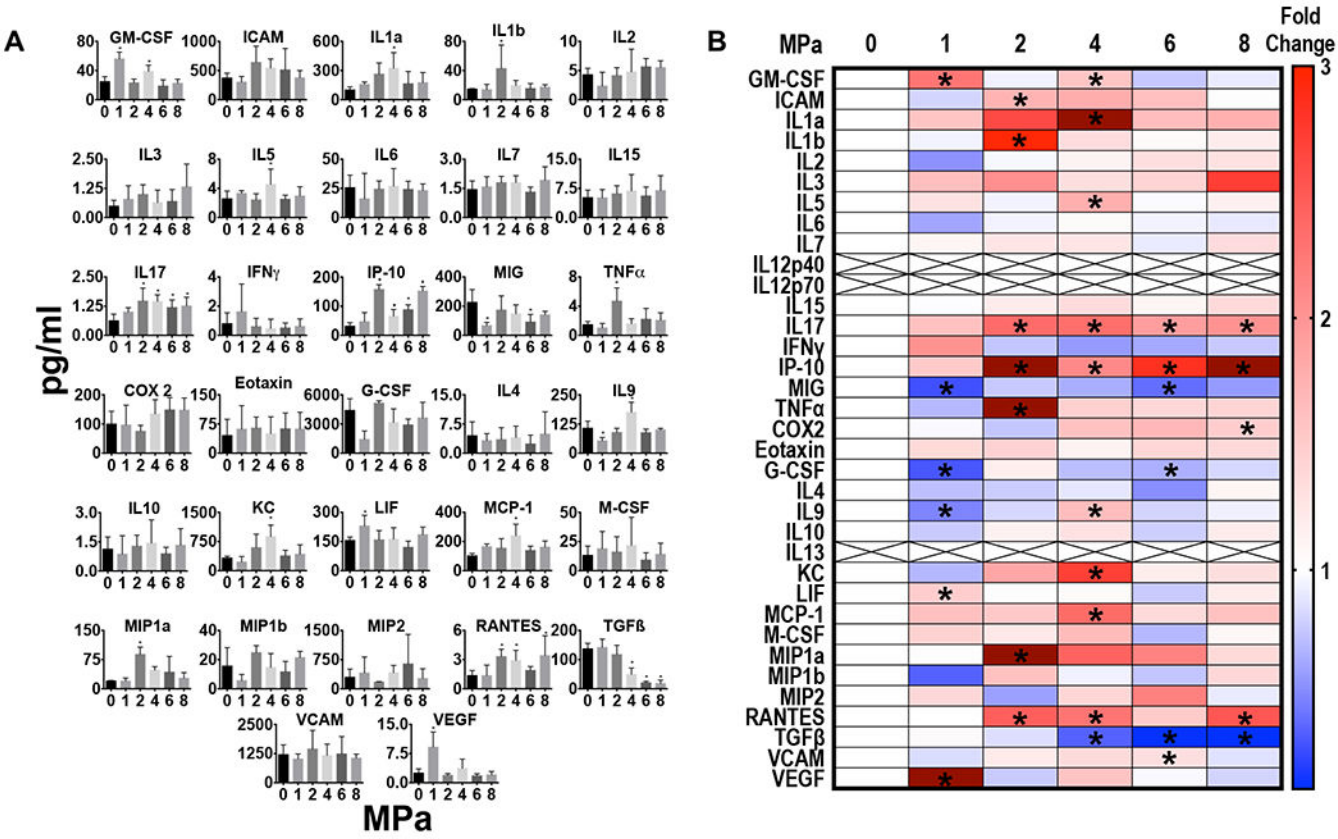

Figure 1.

Hematoxylin and Eosin (H&E) stain of 4T1 (A,B,E,F) and B16 (C,D, G, H) of macroscopic (scale bar =2mm A,B; scale bar 1mm C,D) and high power view of tumors (scale bar = 100μm) G and H 100μm E,F) treated with 0MPa or 6MPa. Areas of hemorrhage and necrosis are seen in the tumors that were either untreated or treated with pFUS.

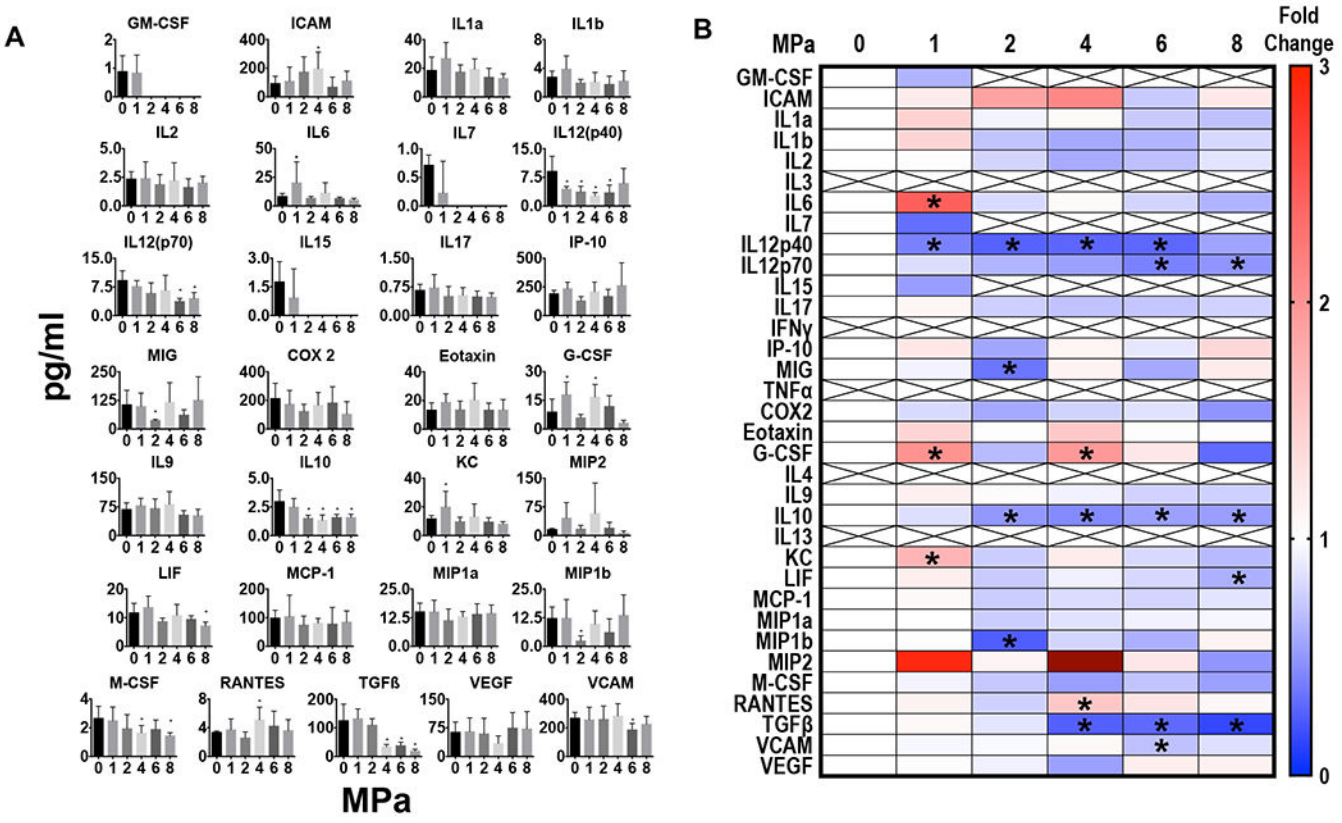

Figure 2.

Immunofluorescent TUNEL stain for DNA damage in B16 (A and B) and 4T1 (D and E) tumors. Quantitative analysis of fluorescence from TUNEL positive cells (green) for B16 (C) and 4T1 (F) demonstrate significant increase at pFUS PNP ≥ 6MPa. DAPI= Blue, TUNEL = Green, Scale bars A, D and B 100μm, B = 200μm. * $p<0.05$ based on ANOVA with multiple comparisons to PNP = 0MPa.

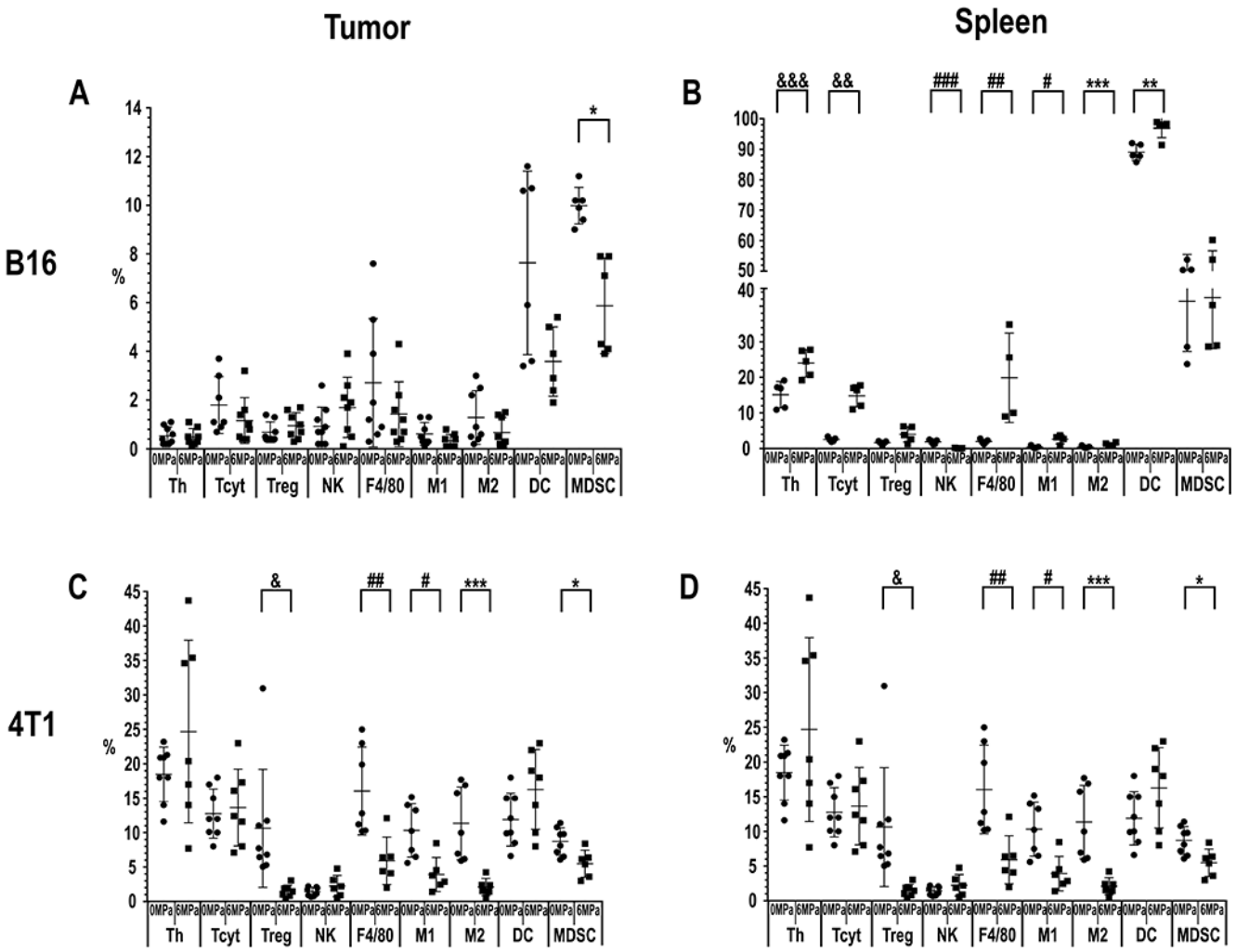

Figure 3.

Proteomic in B16 melanoma following pFUS at 1,2,4,6, and 8 MPa (n=5/PNP). (A) Quantitation of CCTFs and CAM in B16 tumors 24 hours after pFUS exposure at various PNP in picograms/ml or nanograms/ml with x axis in MPa. For 0MPa tumors were not sonicated but considered sham controls. (B) Heat map depicting fold changes in CCTF and CAM at various PNP. Protein levels were quantified by ELISA and fold changes were normalized to sham controls. Significant differences were determined by ANOVA corrected to multiple comparison to PNP= 0MPa with p value <0.05.

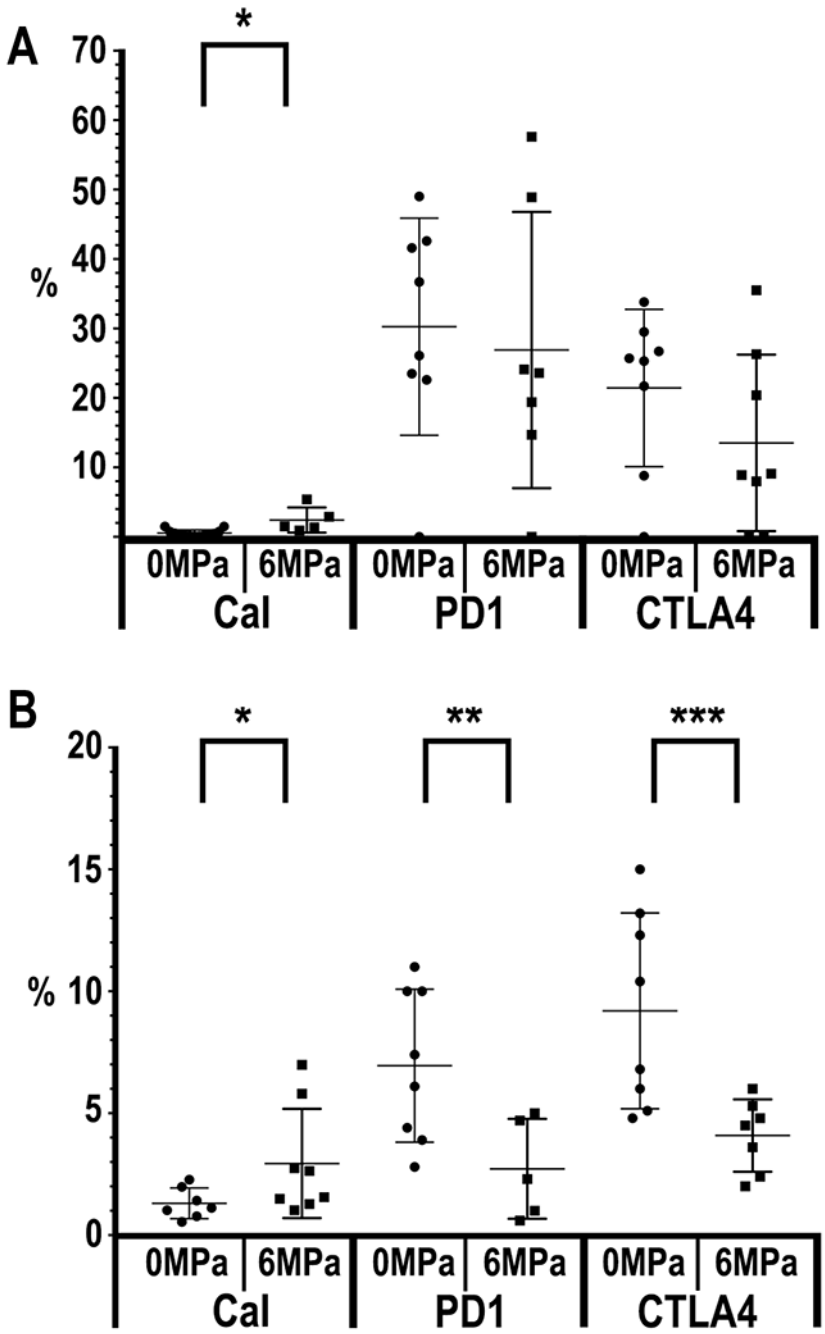

Figure 4.

Proteomic in 4T1 breast cancer following pFUS at 1,2,4,6, and 8 MPa (n=5/PNP). (A) Quantitation of CCTFs and CAM in 4T1 tumors 24 hours after pFUS exposure at various PNP in picograms/ml or nanograms/ml with x axis in MPa. For 0MPa tumors were not sonicated but considered sham controls. (B) Heat map depicting fold changes in CCTF and CAM at various PNP. Protein levels were quantified by ELISA and fold changes were normalized to sham controls. Significant differences were determined by ANOVA corrected to multiple comparison to PNP= 0MPa with p value <0.05.

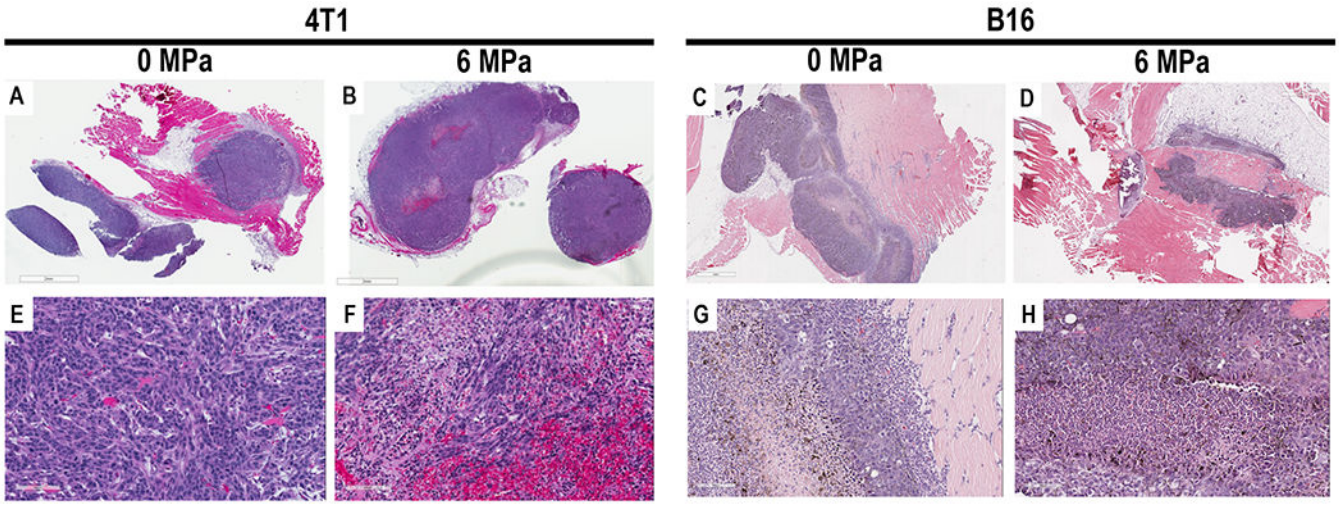

Figure 5.

Graphs of percentage (%) of each phenotype of immune cell population determined flow cytometry analysis (FACS; n=5 mice (10 tumors and 5 spleens)/PNP). FACS results for each tumor or spleen harvested 24 hours following pFUS at PNP = 6MPa compared to tumors that were not sonicated (PNP=0MPa). (A) B16 Tumor: MDSC *p=0.0022 and (B) spleens from mice with B16 tumors: Th &&&p=0.0079, Tcyt &&p=0.0079, NK cells ###p=0.0079, F4/80 macrophages ##p=0.0159, M1 macrophages #p=0.0317, M2 macrophages ***p= 0.0397, DC **p= 0.0317, and MDSC *p=0.02. (C) 4T1 Tumors: Treg &p=0.02, F4/80 ##p=0.02, M1 #p=0.02 and M2 macrophages ***p=0.02 and MDSC *p=0.02. (D) Spleen from mice with 4T1 tumors: Tcyt &&p=0.028, NK ###p=0.028, DC **p=0.028, and MDSC *p=0.028.

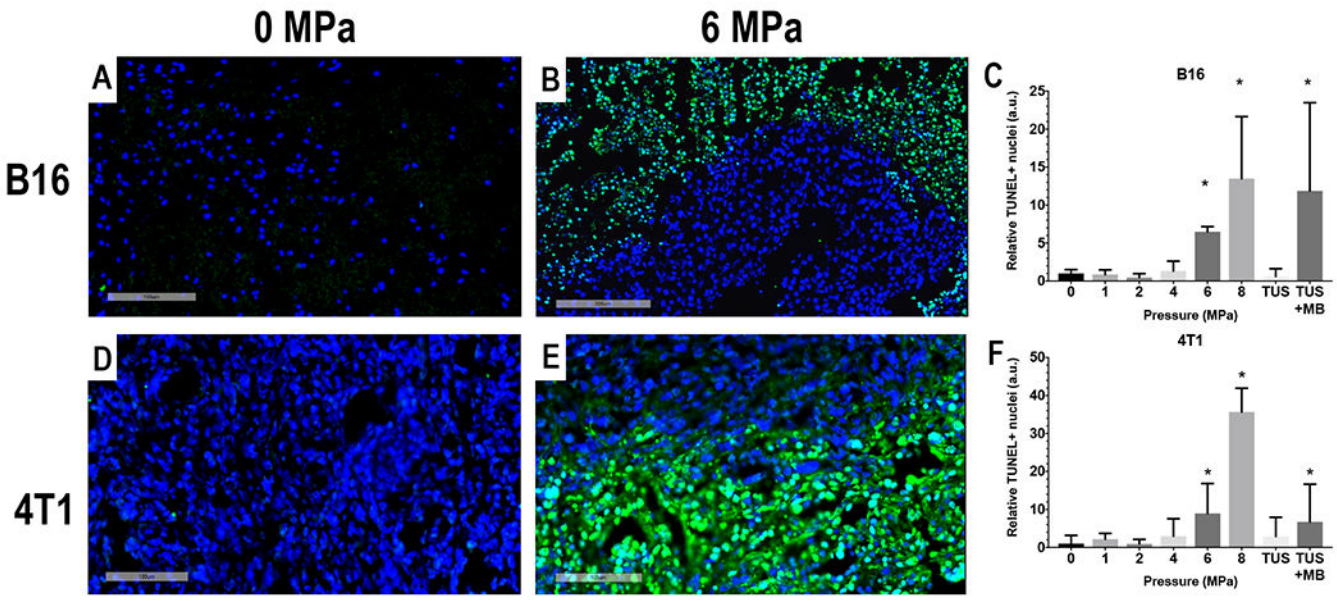

Figure 6.

Graphs of percentage (%) by FACS (n=5 mice (10 tumors and 5 spleens)/PNP) of Calreticulin (Cal), PD1 and CTLA4 expression from either B16 (A) or 4T1 (B) tumors. B16 Cal (p=0.0027) and 4T1 PD1 (p= 0.042) with non-significant trends for decreased CTLA4 (p=0.051) and increased calreticulin (p=0.054).

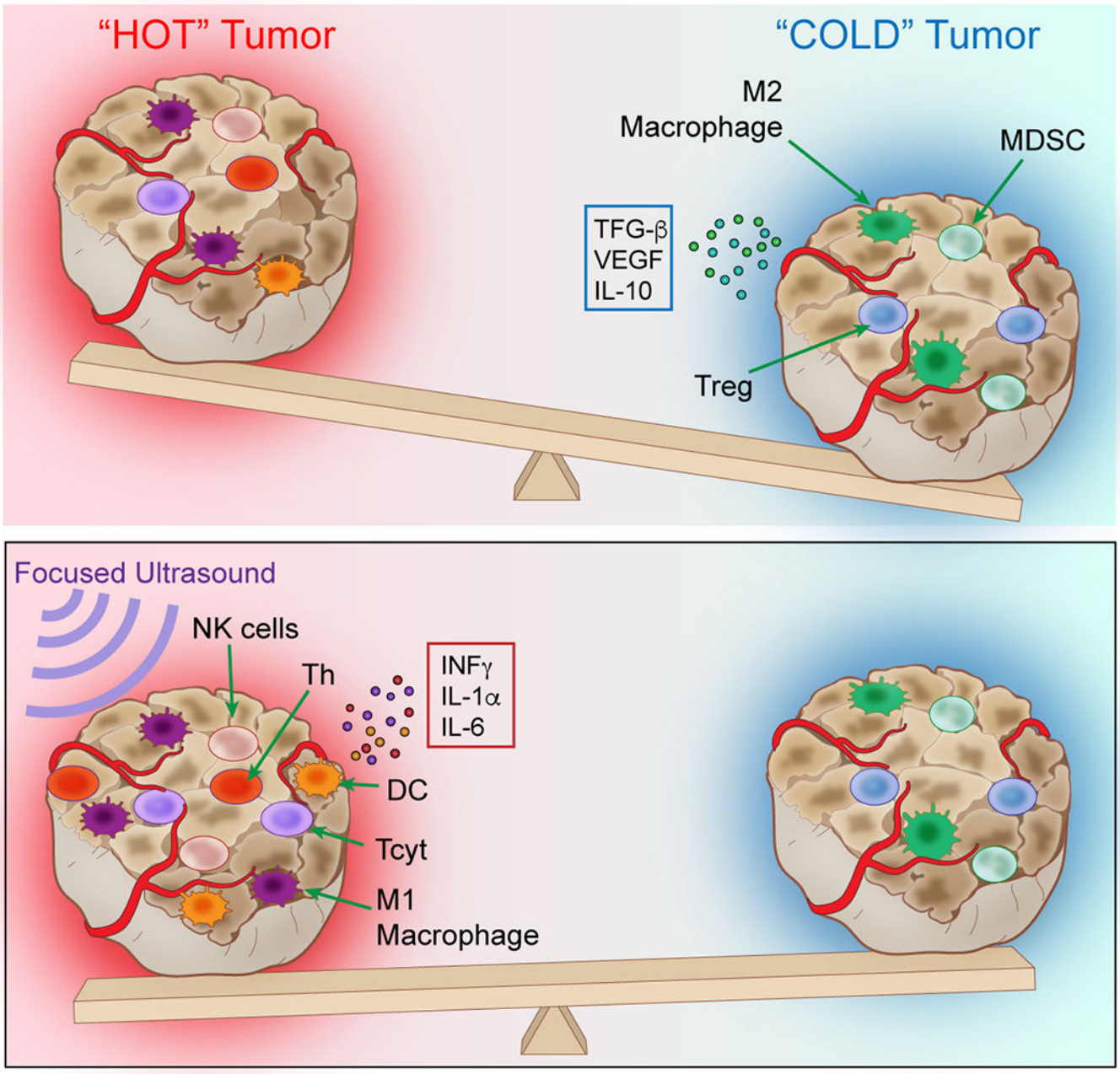

Figure 7.

The balance between intra-tumoral immunosuppressive (cold) and an anti-tumor (hot) tumor microenvironment. The balance between cold and hot TME is dependent on the expression of local concentrations of immune factors (CCTF) in the microenvironment milieu and associated immune cell response. pFUS at >4MPa can start to shift the molecular and cellular balance towards an anti-tumor hot TME within 24 hours and can influence the phenotypes of the local and splenic immune cell populations that could influence treatment effects.